Tuning the Equilibrium Ion Affinity and Selectivity of the EF-Hand Calcium Binding Motif: Substitutions at the Gateway Position†

Steven K. Drake, Keith L. Lee, and Joseph J. Falke*

Department of Chemistry and Biochemistry, University of Colorado, Boulder, Colorado 80309-0215

Received October 10, 1995; Revised Manuscript Received January 26, 1996⊗

ABSTRACT: The ion binding parameters of the EF-hand Ca^{2+} binding motif are carefully tuned for different biological applications. The present study examines the contribution of the ninth position of the Ca^{2+}-coordinating EF-loop to the tuning of Ca^{2+} affinity and selectivity, using the model EF-loop of the *Escherichia coli* galactose binding protein. Eight side chains, representing the entire set of side chains commonly observed in natural EF-loop sequences, are tested at the ninth position of the model EF-loop to determine their effects on equilibrium ion binding parameters. Using the spherical metal ions of groups Ia, IIa, and IIIa and the lanthanides as probes, both the Ca^{2+} affinities and ionic selectivities of the engineered sites are quantitated. Neutral side chains of different size at the ninth EF-loop position [Gln (wild type), Asn, Thr, Ser, Ala, Gly] are observed to yield similar Ca^{2+} affinities and retain the native ability to exclude the physiological competing metal cations Na^+, K^+, and Mg^{2+}. Acidic gateway side chains (Glu, Asp) are found to reduce Ca^{2+} affinity and shift the ionic charge selectivity as much as 10^3-fold toward trivalent cations. Relative to the native Gln, all engineered side chains cause a partial loss of ionic size selectivity, stemming from enhanced affinities for nonphysiological large ions. Overall, the results have implications for the molecular mechanisms used by the EF-loop to control both (i) charge selectivity, which is proposed to stem from the electrostatic repulsion between the coordinating oxygens, and (ii) size selectivity, which is theorized to involve complex interactions between multiple coordinating side chains. Finally, it has recently been shown that the ninth EF-loop position serves as a "gateway" to modulate the kinetics of Tb^{3+} binding and release without shifting the equilibrium affinity of this ion [Drake, S. K., & Falke, J. J. (1996) *Biochemistry 35,* 1753−1760]. The present results confirm that isoelectric substitutions at the gateway position have little effect on Ca^{2+} affinity, thereby supporting the hypothesis that the gateway side chain provides kinetic tuning of Ca^{2+} signaling proteins independently of their Ca^{2+} activation thresholds.

Intracellular Ca^{2+} signaling proteins exhibit Ca^{2+} affinities carefully tuned to match the levels of Ca^{2+} ion generated during a signaling event. In addition, these sites selectively bind Ca^{2+} in the presence of 10^3-10^5-fold higher concentrations of K^+, Na^+, and Mg^{2+}. Such tightly regulated Ca^{2+} affinity and specificity is essential for the activation sites of Ca^{2+} signaling proteins, which must remain "off" until a Ca^{2+} trigger appears, and for Ca^{2+} channel sites, which provide selective Ca^{2+} fluxes [reviewed by Linse and Forsén (1995), Park and MacKinnon (1995), Falke et al. (1994), and Tsien and Tsien (1990)]. The present work focuses on the EF-hand Ca^{2+} binding motif, which is widely used to bind Ca^{2+} ion in eukaryotic cells [Kretsinger & Nockolds, 1973; reviewed by Linse and Forsén (1995), Kawasaki and Kretsinger (1995), Falke et al. (1994), Skelton et al. (1994), Marsden et al. (1990), and Strynadka and James (1989)]. The goal is to identify molecular forces that contribute to EF-hand ion binding affinity and selectivity.

The EF-hand motif possesses a well-characterized architecture. Crystal structures of 45 EF-hand sites reveal a coordinating array of seven oxygens arranged in a pentagonal bipyramidal geometry around the bound Ca^{2+} ion [reviewed by Falke et al. (1994) and Strynadka and James (1989)]. Five of these oxygens arise from a nine-residue EF-loop containing a conserved γ-turn, while the remaining two oxygens stem from the bidentate carboxylate of a glutamate located outside the loop, typically three residues from the loop C-terminus. Access to the ion binding cavity of the motif is regulated by the ninth EF-loop position, whose side chain projects into the shortest pathway connecting the ion binding cavity to solvent (see Figure 1). This "gateway" position controls the kinetics of Tb^{3+} binding and release in engineered EF-loops (Drake & Falke, 1996; Renner et al., 1993), and in natural EF-hand sites the identity of the gateway side chain is correlated with Ca^{2+} kinetics ranging from very slow in Ca^{2+} buffering proteins to quite fast in Ca^{2+} signaling proteins (Drake & Falke, 1996; Falke et al., 1994). The potential role of the gateway side chain in controlling the equilibrium properties of the EF-hand motif, however, remains unclear.

Two key equilibrium parameters of the EF-hand motif are (a) its affinity for Ca^{2+}, and (b) its selectivity for Ca^{2+} relative to other cations. The motif binds spherical metal cations from groups Ia, IIa, and IIIa and the lanthanides, which together provide a set of probe ions differing in charge and size. Studies utilizing these probes have mapped out the Ca^{2+} affinities and selectivities of EF-hand ion binding

† Support Provided by NIH Grant GM48203.

* Corresponding author. Telephone 303-492-3503. Fax: 303-492-5894. E-mail: falke@colorado.edu.

⊗ Abstract published in *Advance ACS Abstracts,* May 1, 1996.

S0006-2960(95)02430-5 CCC: $12.00

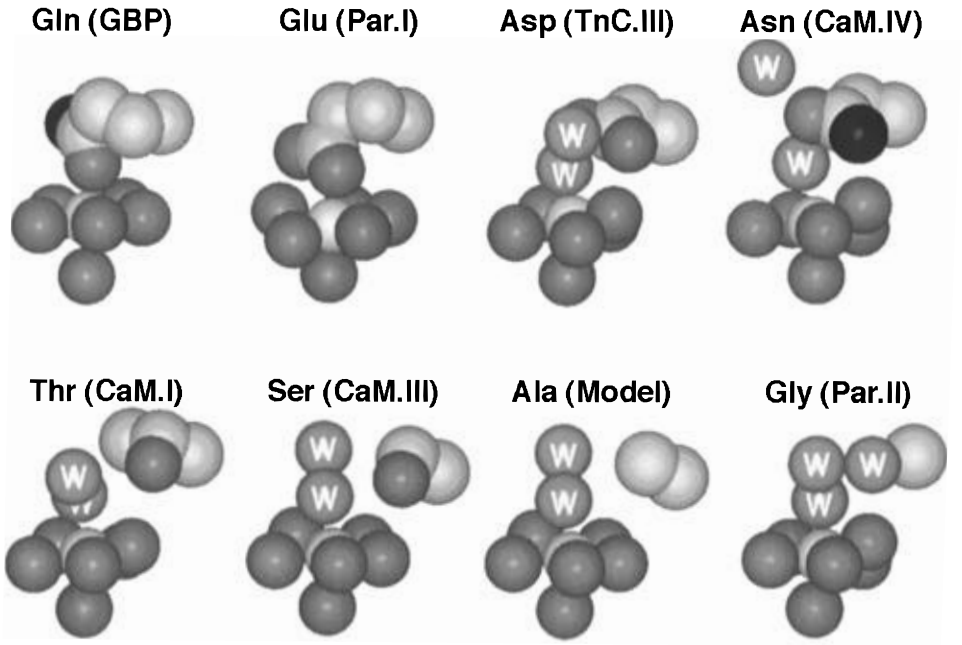

FIGURE 1: Structures illustrating the gateway side chain in different EF-hand sites. Shown are representative EF-hand Ca^{2+} coordination motifs from crystallographic or modeled protein structures. Each site possesses seven protein (dark gray) or solvent water (W) oxygens surrounding the bound Ca^{2+} ion (center). All of the sites are identically oriented, with the shortest pathway for Ca^{2+} dissociation leading upward. Highlighted are the gateway side chains bordering the Ca^{2+} dissociation pathway, provided in each case by the ninth EF-loop position. Shading denotes atom type: black (nitrogen), dark gray (oxygen), light gray (carbon or Ca^{2+}). Seven of the structures are from crystallographic coordinates: the native galactose binding protein site (Gln) (Vyas et al., 1987); site I of parvalbumin (Glu) (Kumar et al., 1990); site III of skeletal troponin C (Asp) (Herzberg & James, 1988); site IV of calmodulin (Asn) (Babu et al., 1988); site I of calmodulin (Thr) (Ban et al., Protein Data Bank, Brookhaven); site III of calmodulin (Ser) (Chattopadhyaya et al., 1992); and site II of parvalbumin (Gly) (Kumar et al., 1990). The Ala gateway was modelled by removing the Ser hydroxyl from site III of calmodulin, because such a gateway has not yet been crystallographically described.

cavities with unusually high resolution [reviewed by Linse and Forsén (1995), Falke et al. (1994), and Horrocks and Albin (1984)]. Such studies reveal that the EF-hand can recognize specific substrate ions on the basis of both their charge and radius (Brito et al., 1991; Snyder et al., 1990; Wang et al., 1984; Chao et al., 1984; Williams et al., 1984; Corson et al., 1983).

The present study utilizes the model EF-hand site of the *Escherichia coli* galactose binding protein (GBP). This model site, which functions to stabilize the folded structure of GBP, consists of a standard nine-residue EF-loop and a coordinating glutamate side chain located, as in other EF-hand motifs, outside the loop (Vyas et al., 1987). The GBP molecule, however, lacks the multisite, cooperative ion binding of typical eukaryotic EF-hand proteins; thus ion binding to GBP can be quantitatively analyzed in terms of a simple, nonallosteric, independent binding site (Vyas et al., 1989; Snyder et al., 1990). Furthermore, spectroscopic detection of metal binding to the GBP site is made possible by an intrinsic tryptophan side chain (Trp 127) whose indole ring is positioned less than 5 Å from the bound metal ion (Vyas et al., 1987; Snyder et al., 1990).

Altogether, the study examines eight different gateway side chains in the context of the model GBP EF-loop, including the seven gateway side chains most commonly observed in natural EF-hands (Asp, Ser, Thr, Glu, Asn, Gly, Gln, in order of decreasing prevalence), as well as one gateway not yet observed in nature (Ala; Falke et al., 1994). A crystal structure is available only for the native GBP site (Vyas et al., 1987), in which the gateway side chain is glutamine, but structures of other EF-hand proteins illustrate a plausible conformation for each engineered gateway region, as summarized in Figure 1.

The capacity of the gateway side chain to tune equilibrium EF-hand parameters is revealed by the effects of gateway substitutions on the ion binding affinity and selectivity of the GBP site. Neutral side chains are found to yield similar Ca^{2+} affinities and have little effect on the selectivity for Ca^{2+} over other physiological metal cations. Acidic side chains, by contrast, are observed to significantly shift the equilibrium charge selectivity of the site toward trivalent ions. Moreover, each of the eight gateway side chains exhibits an altered size selectivity profile for large, nonphysiological cations. Together, these results have important implications for the molecular mechanisms underlying the ionic charge and size selectivities of the EF-hand motif.

MATERIALS AND METHODS

Construction and Isolation of Engineered Proteins. The wild-type and engineered GBP molecules utilized in this study were constructed, isolated, and characterized as described elsewhere in detail (Drake & Falke, 1996).

Quantitation of Metal Binding Equilibria. For each wild-type or engineered protein, binding free energies were determined for the metal cations of groups Ia, IIa, and IIIa and the lanthanides using previously published methods (Drake & Falke, 1996; Falke et al., 1991; Snyder et al., 1990). Briefly, a selected protein (2.5 μM) was equilibrated with a fixed concentration of Tb^{3+} (25 μM), thereby loading its EF-hand site with this phosphorescent lanthanide. Subsequently, sensitized Tb^{3+} phosphorescence triggered by energy transfer from Trp 127 to bound Tb^{3+} was monitored (λ_{ex} = 292 nm, λ_{em} = 543 nm) while a competing metal ion was titrated into the system by stepwise addition. The competing metal displaced bound Tb^{3+}, yielding a corresponding decrease in

the sensitized Tb^{3+} phosphorescence. The resulting plot of bound Tb^{3+} phosphorescence against the concentration of free competing metal [Me] was best fit to the independent site model

$$I/I_{max} = 1 - \{[Me]/(K_{DappMe} + [Me])\} \quad (1)$$

where I/I_{max} is the intensity of the bound Tb^{3+} phosphorescence relative to that in the absence of competing metal ion, [Me] is the concentration of the free competing ion, and K_{DappMe} is the apparent dissociation constant for the competing ion. The nonlinear least-squares, best fit apparent dissociation constant provided by eq 1 was then corrected for competition with Tb^{3+} to yield the true dissociation constant given by

$$K_{DMe} = K_{DappMe}/(1 + [Tb^{3+}]/K_{DTb}) \quad (2)$$

where K_{DMe} is the dissociation constant for metal ion in the absence of Tb^{3+} ion, K_{DTb} is the dissociation constant for Tb^{3+} ion, and $[Tb^{3+}]$ is the free Tb^{3+} ion concentration. Finally, the dissociation constant was converted to the binding free energy according to

$$\Delta G^{\circ}_{Me} = RT \ln K_{DMe} \quad (3)$$

for 1 M standard state concentrations. All measurements were at 25° C in 100 mM KCl and 10 mM PIPES, pH 6.0 with KOH.

The free ion concentrations were determined as previously described (Drake & Falke, 1996; Falke et al., 1991). The Tb^{3+} dissociation constant K_{DTb} was also measured as described elsewhere in detail, including a recently improved technique for quantitating Tb^{3+} binding to sites with higher-than-native affinities (Drake & Falke, 1996). In all calculations, molar concentrations, rather than activities, were used. This approximation introduces a nonrandom error into the ΔG°_{Me} values of interest; however, this error is relatively small since the relevant experimental conditions yield activity coefficients of the same order as unity, ranging between $0.5 \leq \gamma \leq 1.0$ for monovalent, divalent, and trivalent ions (Harned & Owen, 1950). Thus, activity corrections would shift the ΔG°_{Me} values of Figures 2−4 by less than 0.2 kcal mol^{-1}.

Error Determination. The error range (Z) of each ΔG°_{Me} measurement was calculated from the relationship

$$Z = RT \ln (K_{DMe} \pm 1 \text{ standard deviation}) \quad (4)$$

where the standard deviation of K_{DMe} was determined by the percentage error in K_{DappMe} or K_{DTb}, whichever was larger. Since most errors were negligibly small on the log scale of free energy, Figures 2−4 present only the largest error for each data set.

Molecular Graphics. Images of EF-hand binding sites were generated by Insight II graphics software (Version 2.3.5; Biosym) running on a Silicon Graphics Personal Iris 4D/35. Structural coordinates were obtained from the Protein Data Bank (Brookhaven).

RESULTS

Strategy. To investigate the contribution of the gateway position to the equilibrium ion binding affinity and selectivity of the EF-hand motif, the present work compares eight different gateway side chains in the model EF-hand site of GBP. Included are the native gateway residue, a glutamine (Q142), and seven other side chains differing in size or charge: glutamate (Q142E), aspartate (Q142D), asparagine (Q142N), threonine (Q142T), serine (Q142S), alanine (Q142A), and glycine (Q142G). Together, these eight gateway side chains represent the entire set of experimentally accessible gateway residues in GBP, since other gateway substitutions have been shown to block GBP expression (Drake & Falke, 1996). The study also characterizes two negative control substitutions at a noncoordinating position, namely, the fourth EF-loop position, at which the surface-exposed lysine side chain is replaced by arginine or glycine (K137R and K137G, respectively).

The resulting 10 GBP molecules, which were previously used to examine the kinetic tuning role of the gateway side chain, have been shown to be stable, well-folded proteins. Their predicted molecular masses have been confirmed by mass spectrometry; in addition, their native function, stability, and conformation has been verified by galactose affinity measurements, thermal melting profiles, and ^{19}F NMR studies, respectively (Drake & Falke, 1996). The only significant effect was a 5 ± 1 °C decrease in T_m observed for all seven gateway substitutions, consistent with the proposed function of the GBP Ca^{2+} binding site in protein stabilization rather than signaling (Drake & Falke, 1996; Vyas et al., 1987). Outside the region of their engineered EF-loops, the mutant proteins appeared to be identical to the wild-type molecule. The two control mutants were indistinguishable from wild type in all measurements.

To probe the equilibrium ion binding parameters of these proteins, the present study measured metal binding affinities using a sensitized Tb^{3+} phosphorescence method that has proven useful in a number of Ca^{2+} binding proteins (Burroughs et al., 1994; Cronce & Horrocks, 1992; Snyder et al., 1990; Evans, 1990; Horrocks & Albin, 1984; Brittain et al., 1976). In GBP, this method makes use of the indole ring of Trp 127, which lies within 5 Å of the bound metal ion. When Tb^{3+} is bound, electronic excitation of the indole results in transfer of the excited state to the metal, yielding selective excitation of the Tb^{3+} population bound in the site. The resulting phosphorescence emission of this population effectively monitors the Tb^{3+} occupancy of the EF-hand. Subsequently, the binding of any other metal ion can be detected as a decrease in the bound Tb^{3+} emission when the competing metal is titrated into the site. The true equilibrium dissociation constant (K_D) for the competing metal is determined by both (i) its ability to displace Tb^{3+} and (ii) the Tb^{3+} affinity of the empty site (see Materials and Methods).

For each site, equilibrium dissociation constants have been measured for the metal cations of groups Ia, IIa, and IIIa and the lanthanides. These cations, which are catalogued in Table 1, possess filled outer electronic subshells and thus exhibit highly ionic coordination with little or no preference for a specific coordination geometry. As a result, they can be regarded as simple, hard spheres of incrementally varying charge and size, suitable for probing the charge and size discrimination of the EF-hand metal binding cavity (Snyder et al., 1990).

Using these probe ions, the equilibrium affinity and selectivity parameters of the wild-type and engineered molecules have been measured and compared, yielding the

Table 1: Summary of Probe Metal Ions

metal ion	effective ionic radius (Å)[a]	native K_D (M)[b]
group Ia		
Li^+	0.84	≥6
Na^+	1.12	≥3
K^+	1.46	≥4
Rb^+	1.56	≥3
group IIa		
Mg^{2+}	0.81	$(1.2 \pm 0.2) \times 10^{-2}$
Ca^{2+}	1.06	$(1.4 \pm 0.1) \times 10^{-6}$
Sr^{2+}	1.21	$(1.9 \pm 0.1) \times 10^{-4}$
Ba^{2+}	1.38	$(1.2 \pm 0.4) \times 10^{-2}$
group IIIa		
Sc^{3+}	0.81	$(5 \pm 2) \times 10^{-6}$
Y^{3+}	0.96	$(1.3 \pm 0.1) \times 10^{-6}$
La^{3+}	1.10	$(7.1 \pm 0.5) \times 10^{-5}$
lanthanides		
Lu^{3+}	0.92	$(5.5 \pm 0.4) \times 10^{-7}$
Yb^{3+}	0.925	$(4.7 \pm 0.5) \times 10^{-7}$
Tm^{3+}	0.94	$(7 \pm 1) \times 10^{-7}$
Er^{3+}	0.945	$(7.3 \pm 0.2) \times 10^{-7}$
Ho^{3+}	0.96	$(1.0 \pm 0.1) \times 10^{-6}$
Dy^{3+}	0.97	$(1.0 \pm 0.1) \times 10^{-6}$
Tb^{3+}	0.98	$(2.0 \pm 0.5) \times 10^{-6}$
Gd^{3+}	1.00	$(4.3 \pm 0.2) \times 10^{-6}$
Eu^{3+}	1.01	$(3.3 \pm 0.2) \times 10^{-6}$
Sm^{3+}	1.02	$(6.0 \pm 0.4) \times 10^{-6}$
Nd^{3+}	1.05	$(2.1 \pm 0.2) \times 10^{-5}$
Pr^{3+}	1.06	$(1.8 \pm 0.2) \times 10^{-5}$
Ce^{3+}	1.07	$(3.4 \pm 0.3) \times 10^{-5}$

[a] Effective ionic radius for 7-fold coordination (Snyder et al., 1990; Shannon, 1976) [b] Equilibrium dissociation constant for the binding of the indicated ion to the native EF-loop site of the *E. coli* galactose binding protein. Conditions: 25 °C, 2.5 μM protein, 100 mM KCl, 10 mM PIPES, pH 6.0.

results described below. Our study includes three previously characterized mutants, Q142E, Q142D, and Q142N (Falke et al., 1991), because improvements in the Tb^{3+} competition assay (see Materials and Methods) have provided new, more accurate data for these proteins.

Equilibrium Ion Binding Parameters of the Native Site. As a standard of comparison, the spherical ion affinities of the native site have been redetermined and are summarized in Table 1. The Ca^{2+} dissociation constant of the native site is $K_D = 1.4 \pm 0.1$ μM, placing this site in the moderate category of Ca^{2+} affinities exhibited by the EF-hand superfamily (Linse & Forsén, 1995; Falke et al., 1994).

With regard to other metals, the native site exhibits the capacity to discriminate between cations of different charge and size. The site essentially excludes the monovalent ions of Group Ia (Li^+, Na^+, K^+, Rb^+; in order of increasing radius), which all yield large dissociation constants satisfying $K_D \geq 3$ M [Snyder et al., 1990; also Drake and Falke (data not shown)]. In contrast, the site exhibits high affinity binding for selected divalent and trivalent cations from group IIa (Mg^{2+}, Ca^{2+}, Sr^{2+}, Ba^{2+}), group IIIa (Sc^{3+}, Y^{3+}, La^{3+}), and the lanthanides (Lu^{3+}, Yb^{3+}, Tm^{3+}, Er^{3+}, Ho^{3+}, Dy^{3+}, Tb^{3+}, Gd^{3+}, Eu^{3+}, Sm^{3+}, Nd^{3+}, Pr^{3+}, Ce^{3+}), where the affinity varies with ionic size.

Figures 2A and 3A summarize the ionic size selectivity of the wild-type site as free energy profiles for divalent and trivalent ions, respectively. These profiles plot binding free energy as a function of the effective ionic radius, yielding a free energy well that signifies the existence of an optimal ionic radius for binding to the site. Although the precise value of this radius is undetermined due to the limited set of metal ion radii available, it is clear that the optimal radius for divalent ions approximately matches the size of Ca^{2+} (Figure 2A). Overall, the divalent ions, which differ greatly in size but are few in number, provide a wide-range, low resolution free energy profile, while the trivalent ions provide a narrow, higher resolution view of the free energy profile in the vicinity of the optimal radius.

Effect of Gateway Substitutions on Ca^{2+} Affinity. Table 2 presents the Ca^{2+} affinities of the wild-type and engineered proteins. Notably, the altered EF-loops possessing a neutral side chain at the gateway position (Gln, Asn, Thr, Ser, Ala, Gly) exhibit similar affinities for Ca^{2+}, all within 4-fold that of the native site. An analogous result was previously obtained for Tb^{3+} affinities, which varied less than 3-fold for the same set of neutral gateway side chains (Drake & Falke, 1996).

Acidic side chains at the gateway position (Glu, Asp), by contrast, are observed to significantly decrease Ca^{2+} affinity (Table 2). In particular, the glutamate and aspartate side chains yield 300- and 16-fold lower Ca^{2+} affinities than the native glutamine, respectively. These decreased affinities for the divalent Ca^{2+} ion, which stem from a shift in the charge selectivity of the site (see below), demonstrate that changes in the charge of the gateway side chain can alter equilibrium Ca^{2+} affinity.

Effect of Neutral Gateway Substitutions on Ion Selectivity. When the glutamine at the gateway position is substituted with other neutral side chains (Asn, Thr, Ser, Ala, Gly), the resulting engineered sites retain the native charge selectivity. Like the wild-type site, these sites exclude monovalent ions ($K_D \geq 3$ M, data not shown) but bind divalent and trivalent ions in a size-selective manner (Figure 2 and 3). Thus neutral gateway substitutions do not significantly alter the charge discrimination parameters of the ion binding cavity.

The engineered neutral side chains do, however, generate detectable changes in the ionic size selectivity of the site. For divalent ions, the size selectivities of the native and engineered sites are compared in Figure 2. Each of the neutral gateway side chains yields a divalent ion free energy well similar in depth and position to that of the wild-type site, with an optimal radius near that of Ca^{2+} ion. The most conservative neutral substitution, asparagine, yields a divalent ion free energy well indistinguishable from that of the native glutamine (Figure 2B), while the other neutral side chains produce discernable differences. The most striking changes are observed for threonine and serine, which yield native affinities for the three smallest divalents (Mg^{2+}, Ca^{2+}, Sr^{2+}) but significantly higher-than-native affinities for Ba^{2+} (increased 42- and 180-fold, respectively; Figure 2C,D), indicating that the threonine and serine gateway side chains allow greater stabilization of this large ion. More subtle effects are seen for the alanine and glycine substitutions, which slightly decrease the steepness of the divalent ion free energy well in the large ion limit (slopes are 70% and 84% that of the wild type well, respectively, as determined by the Ca^{2+}, Sr^{2+}, and Ba^{2+} ions; Figure 2E,F). It follows that these substitutions increase the ability of the ion binding cavity to accommodate large ions.

All of the engineered neutral side chains alter the size selectivity of trivalent ion binding, as revealed by the trivalent ion free energy profiles shown in Figure 3. As observed for divalent ions, the conservative asparagine substitution yields the free energy profile closest to that of wild type

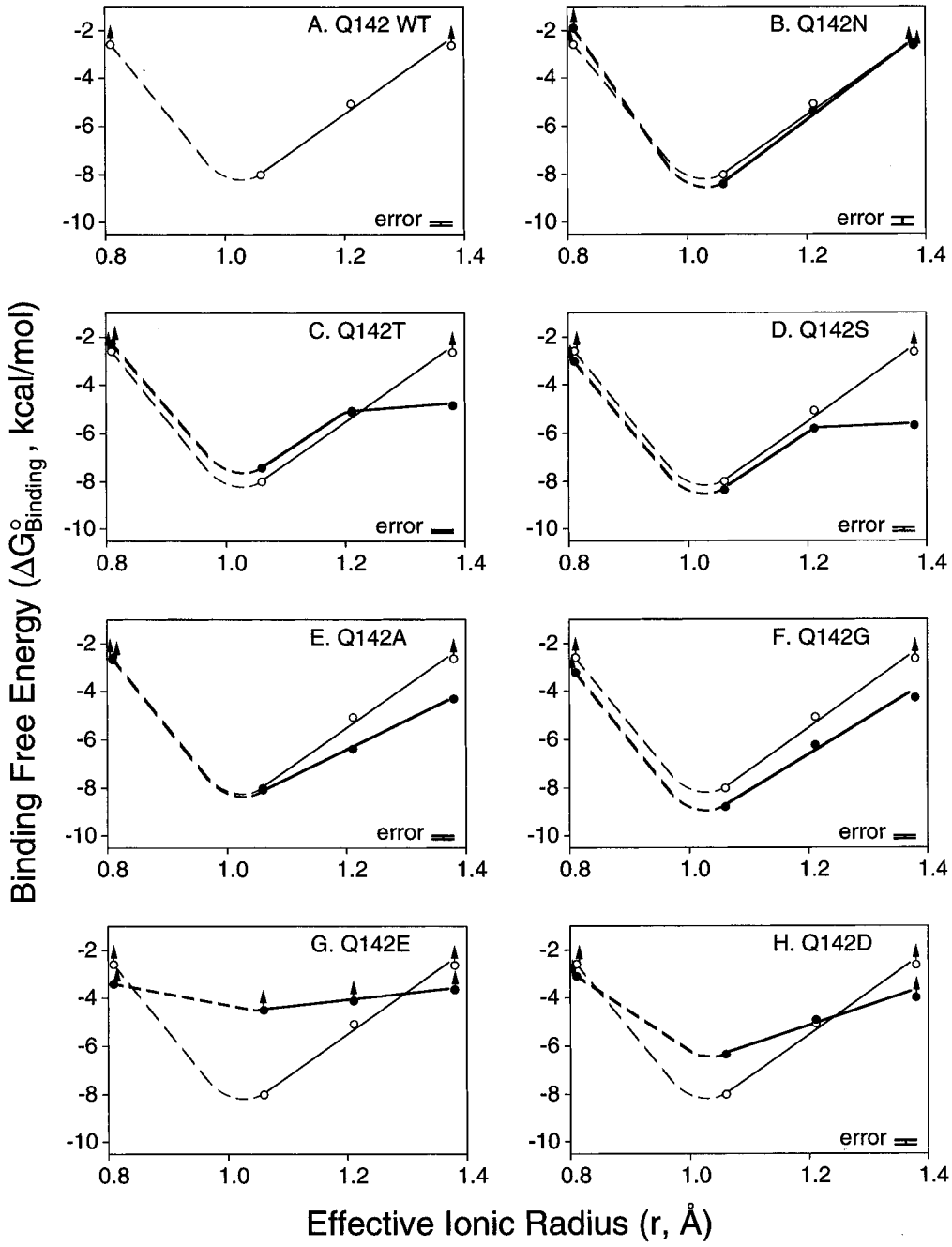

FIGURE 2: Binding free energy as a function of divalent cation size: effect of gateway substitutions. Plotted against effective ionic radius are binding free energies for divalent cations of Group IIa. Each panel shows data for the native site (open circles, fine curve) and, excepting the first panel, for a site possessing an engineered gateway side chain at the ninth EF-loop position (filled circles, bold curve). An error bar is indicated for the largest error in each data set, calculated as RT ln($K_D \pm 1$ standard deviation). Effective ionic radii are for 7-fold coordination, from Shannon (1976). Group IIa cations utilized were, in order of increasing radius, Mg^{2+}, Ca^{2+}, Sr^{2+}, and Ba^{2+}. Dashed curves indicate regions of the free energy profile which are incompletely determined by the available radii. Lower limits (up arrows) are indicated for ions which yielded less than 50% displacement of Tb^{3+} at their maximum attainable concentrations in the Tb^{3+} competition assay (see Materials and Methods). All measurements were at 25 °C with 2.5 μM protein, 100 mM KCl, and 10 mM PIPES, pH 6.0.

(Figure 3B). However, each of the neutral gateway substitutions, including asparagine, introduces a new local minimum into the free energy profile that is centered at a radius between 1.00 and 1.05 Å. For the threonine, serine, and alanine gateway residues, the new local minimum also appears to be a global minimum, representing an increase in radius of the optimal substrate ion by at least 0.1 Å (Figure 3C−E). For the asparagine and glycine gateway residues, two local minima are observed in the free energy profile, one near the original optimal radius of the native site and the second at the new, larger radius (Figure 3B, F). The absence of the latter local minimum in the native profile indicates that the native gateway glutamine prevents the formation of an alternative stable structure for the binding of large ions.

Effect of Acidic Gateway Subsitutions on Ion Selectivity. The most dramatic changes in the charge selectivity of the model EF-hand are observed when the two acidic side chains, glutamate and aspartate, are substituted at the gateway position. The engineered glutamate gateway decreases the optimal divalent affinity 300-fold and increases the optimal trivalent affinity 6-fold, representing an overall 10^3-fold shift in the charge selectivity from divalent to trivalent ions (Figures 2G and 3G). Similarly, the aspartate gateway

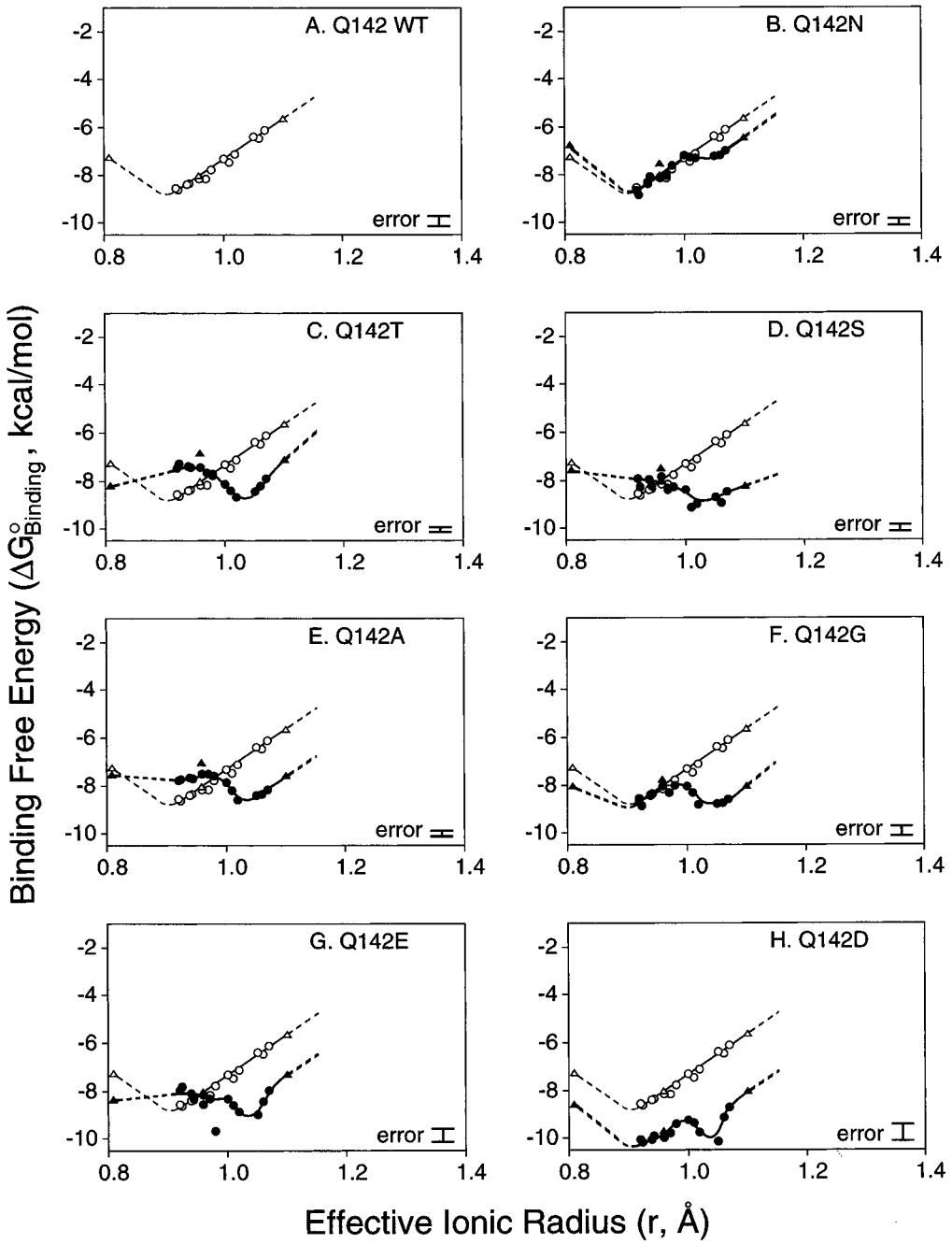

FIGURE 3: Binding free energy as a function of trivalent cation size: effect of gateway substitutions. The legend is as for Figure 2, except that the indicated binding free energies are for trivalent cations from group IIIa (triangles) and the lanthanides (circles). In order of increasing radius, these were Sc^{3+}, Lu^{3+}, Yb^{3+}, Tm^{3+}, Er^{3+}, Ho^{3+}, Y^{3+}, Dy^{3+}, Tb^{3+}, Gd^{3+}, Eu^{3+}, Sm^{3+}, Nd^{3+}, Pr^{3+}, Ce^{3+}, and La^{3+}.

reduces the optimal divalent affinity 17-fold and increases the optimal trivalent affinity 13-fold, yielding a 10^2-fold enhanced selectivity for trivalent ions (Figures 2H and 3H). These results demonstrate that the electrostatic properties of the gateway side chain contribute to the charge selectivity of the EF-hand motif.

The acidic gateway substitutions also alter the size selectivity of the motif. For divalent ions, the glutamate and aspartate substitutions significantly reduce the steepness of size selectivity in the large ion limit, thereby decreasing the slope of the free energy profile 6- or 2-fold, respectively (Figure 2G, H). For trivalent ions, a new local minimum is found at the same radius observed for neutral side chain substitutions (Figure 3G, H). Overall, acidic gateway side chains significantly decrease the size selectivity of the site, indicating a more adjustable ion binding cavity that can more easily accommodate ions of different radii.

Control Substitutions. In contrast to substitutions at the gateway position of the EF-loop, the two control substitutions at the surface-exposed, non-coordinating fourth position of the loop (K137R, K137G) yield wild-type ion binding parameters. Both the Ca^{2+} affinities (Table 2) and ion selectivities of these control sites are indistinguishable from the those of native site (Figure 4). It follows that the altered equlibrium binding parameters observed for the gateway substitutions are not generated by loop substitutions which preserve the native coordination environment.

DISCUSSION

Role of the Gateway Side Chain in the Binding Equilibria of Physiological Ions. Overall, the present study of a model

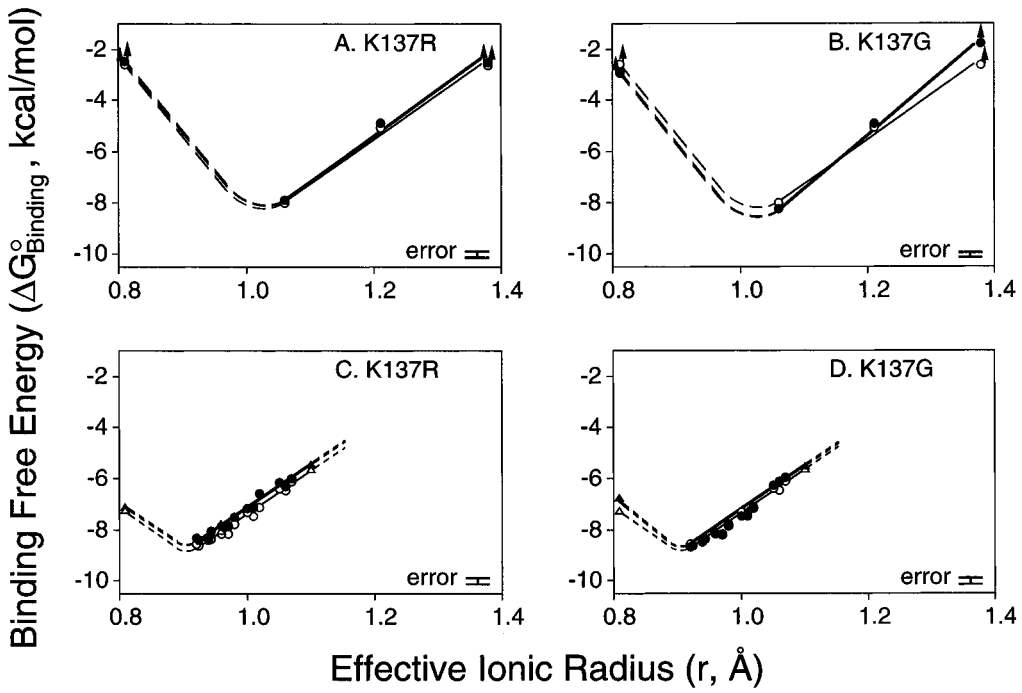

FIGURE 4: Effect of control EF-loop substitutions on size selectivity. The legend as for Figures 2 and 3. Shown are data for two substitutions at the fourth position of the EF loop (K137R, K137G). For each engineered site, the upper panel describes the binding free energies of divalent ions from group IIa, while the lower panel describes the binding free energies of trivalent ions from group IIIa and the lanthanides.

Table 2: Effect of Gateway Substitutions on Ca^{2+} Affinity[a]

site	gateway side chain	Ca^{2+} K_D (μM)
Q142(WT)	Gln	1.4 ± 0.1
K137R	Gln	1.6 ± 0.1
K137G	Gln	0.9 ± 0.1
Q142E	Glu	≥ 500
Q142D	Asp	23 ± 2
Q142N	Asn	0.7 ± 0.1
Q142T	Thr	3.6 ± 0.1
Q142S	Ser	0.7 ± 0.1
Q142A	Ala	1.2 ± 0.1
Q142G	Gly	0.4 ± 0.1

[a] Ca^{2+} binding to the *E. coli* galactose binding protein measured under the following conditions: 25° C, 2.5 μM protein, 100 mM KCl, 10 mM PIPES, pH 6.0.

EF-hand demonstrates that the charge of the gateway side chain, rather than its size or structure, is most strongly coupled to the equilibrium binding of physiological ions. Thus, when the glutamine located at the gateway of the native EF-loop is substituted with another neutral side chain (Asn, Thr, Ser, Ala, Gly; Figure 1), in each case the engineered site retains nearly native Ca^{2+} affinity (within 4-fold that of wild type; Table 2) and retains the ability to exclude the other major physiological cations (Na^+, K^+, and Mg^{2+}; Figure 2). In contrast, when an acidic side chain (Glu, Asp) is engineered into the gateway, the Ca^{2+} affinity of the site is reduced up to 300-fold, due to a shift in ion selectivity from divalent to trivalent ions.

The observation that neutral side chains of different size yield similar Ca^{2+} affinities is consistent with the indistinguishable Ca^{2+} coordination structures of diverse EF-hand sites possessing different gateway side chains. Coordination at the axial ($-X$) position is seen to stem from either (i) a directly coordinating Gln or Glu side chain oxygen, as in the wild-type GBP site, or (ii) a water oxygen which replaces all shorter gateway side chains (Strynadka & James, 1989). The insensitivity of Ca^{2+} affinity to gateway size also confirms an important feature of the gateway hypothesis of kinetic tuning, which proposes that the size of the gateway tunes only the transition state barrier for metal binding and release, with little effect on the binding equilibrium for the physiological ion. Such independent control of kinetics and affinity may enable simultaneous optimization of the speed and threshold of Ca^{2+} activation in Ca^{2+} signaling applications (Drake & Falke, 1996; Renner et al., 1993).

Implications for General Mechanisms of Charge Selectivity. The contrasting abilities of the engineered sites to discriminate between nonphysiological ions of different charge and size is revealed by their binding affinities for the spherical metal ions from groups Ia, IIa, and IIIa and the lanthanides (Table 1 and Figures 2−4). When the native glutamine gateway residue is substituted with a negatively charged side chain, glutamate or aspartate, the charge selectivity of the site is observed to shift 10^3- or 10^2-fold, respectively, from divalent toward trivalent ions (Figures 2G,H and 3G,H). The charge selectivity of the site is not entirely determined by the gateway side chain, however, since many examples of natural sites exist in which high affinity Ca^{2+} binding is provided by gateway glutamate and aspartate residues [reviewed in Falke et al. (1994)]. Thus, the contribution of the gateway side chain to charge selectivity depends on the site context.

The findings strongly support the electrostatic repulsion model for EF-hand charge selectivity (Falke et al., 1991). This model proposes that charge selectivity stems from the strong repulsion between the negatively charged coordinating oxygens, which are in direct, van der Waals contact in the closed conformation of the occupied site. Such charge repulsion must be offset by favorable electrostatic interactions with the bound cation if the occupied site is to be stable. In the native site, for example, the negative charge of the coordinating oxygen array is adjusted so that the singly charged Na^+ and K^+ ions lack sufficient positive charge to

stabilize the contacts between coordinating oxygens, while the greater charge of the Ca^{2+} ion is able to overcome the oxygen−oxygen repulsion. When the inter-oxygen repulsion is increased by substitution of another negative charge into the gateway (or other) position, divalent ions are no longer able to adequately stabilize the coordinating oxygen array, yielding the observed shift in selectivity toward trivalent ions.

Implications for General Mechanisms of Size Selectivity. The native site exhibits an impressive ability to discriminate between ions possessing the same charge but different sizes. When the binding free energies of divalent or trivalent ions are plotted against their ionic radii, the resulting free energy well exhibits a large, positive slope in the large ion limit (Figures 2A and 3A). This slope indicates that the size of the ion binding cavity is constrained by strong mechanical or electrostatic forces, such that large ions must do work against the net constraining force to expand the cavity. The magnitude of this constraining force has been shown to be less than that required to distort covalent bonds, but significantly greater than the constraining force provided by a typical protein interior (Falke et al., 1991; Sandberg & Terwilliger, 1991). At least part of the constraint stems from the architecture of the EF-hand motif, which completely surrounds the bound ion, since other ion binding motifs that fail to engulf the bound ion lack size selectivity (Needham et al., 1993).

The constraints on the cavity size do not, however, depend in a simple way upon the identity of the gateway side chain. For divalent ions, replacement of the native Gln gateway side chain with a shorter side chain does not detectably increase the optimal cavity radius (Figure 2); instead, such substitutions typically reduce the ability to discriminate ions larger than Ca^{2+}. Thus, the Ala and Gly substitutions decrease the slope of the divalent ion size selectivity profile in the large ion limit (Figure 2E,F), indicating that the ion binding cavity has become more flexible. Notably, considerable size selectivity still remains even when the gateway side chain is removed by the latter Gly substitution (Figure 2F), indicating that other elements of the site provide most of the size discrimination for divalent ions. The Thr and Ser substitutions specifically stabilize the large Ba^{2+} ion, suggesting that the β-carbon hydroxyl of these side chains is fortuitously positioned to interact with the Ba^{2+} ion, either directly or by stabilization of a coordinating water molecule (Figures 1 and 2C,D). Interestingly, the divalent ion selectivity profiles of the Thr and Ser mutants are similar to that recently described for the cyclic nucleotide-gated Ca^{2+} channel (Park & MacKinnon, 1995), suggesting that the well-characterized EF-hand motif may be a useful model system for ion channel selectivity.

In the case of trivalent ions, gateway side chains of different size again fail to generate a systematic shift of the optimal radius (Figure 3B−H). Instead, all seven gateway substitutions yield a new local minimum in the trivalent size selectivity profile. This new feature is positioned within a range of atomic radii spanning 1.00−1.05 Å, or approximately 0.1 Å larger than the optimal radius of the native site. For some gateway side chains (Asp, Asn, Gly), the original optimal radius is observed in addition to the new local minimum, indicating that the site can bind two distinct ionic sizes with high affinity. Overall, these results indicate that gateway substitutions enable the site to adopt a new structure when stabilizing large trivalent ions, and that this structure is inaccessible to the native site. The altered structure could change the constraints on the size of the ion binding cavity or could allow an increased coordination number.

Together, the divalent and trivalent size selectivities are consistent with a "side chain interaction" model, in which the size constraints of the ion binding cavity are generated by complex contacts between multiple coordinating side chains. Such contacts include the specific hydrogen-bond interactions known to exist in the EF-hand motif (Strynadka & James, 1989). Additional, nonspecific contacts are provided by the close packing of coordinating side chains. Loss of specific or nonspecific contacts could explain the greater flexibility of the ion binding cavity observed for gateway substitutions which decrease the steepness of the ion size selectivity profiles (Figures 2 and 3). Due to the complexity of interactions between multiple side chains, it appears difficult or impossible to engineer a defined cavity size by rational design methods.

Comparing the ionic size selectivity profiles of the native GBP site with those generated by gateway substitutions, it is apparent that the wild-type Gln gateway yields the maximum size selectivity for both divalent and trivalent metal ions (Figures 2 and 3). All other gateway side chains are observed to decrease size selectivity, primarily by increasing the affinities of the site for divalent and trivalent ions in the large ion limit. The impressive size-selectivity of the native site may be required to avoid the accumulation of toxic metals in the periplasmic compartment, where the free GBP concentration approaches 1 mM (Ames, 1986).

Generality of Gateway Tuning to Other EF-Hand Sites. The literature describes only one other EF-hand protein in which the gateway position has been engineered, namely, the CD site of oncomodulin where the native Asp has been changed to Glu (MacManus et al., 1989; Hapak et al., 1989). This substitution has little or no effect on the Ca^{2+} and Mg^{2+} affinities of the CD site but increases the Lu^{3+} affinity up to 8-fold (Hapak et al., 1989). Such results are fully analogous to those presented here for GBP, where isoelectric substitutions that change only the size of the gateway side chain have little effect on the affinity for Ca^{2+}, Mg^{2+} and other physiological ions but do alter the binding of trivalent ions. Thus, the present conclusion that the size of the gateway side chain is not an important determinant of Ca^{2+} affinity is likely to be a general one among the broad family of EF-hand motifs. Future studies, both in GBP and in other EF-hand proteins, will further test this proposal as well as the other two major conclusions of the present work, namely, that (i) the size constraints on the ion binding cavity stem from complex specific and nonspecific interactions between multiple coordinating side chains while (ii) the charge selectivity of the cavity stems from electrostatic repulsion between the coordinating oxygens.

ACKNOWLEDGMENT

We thank Drs. Olve Peersen and Andrea Hazard for helpful comments, Loree Kim for expert technical assistance, and NIH Grant GM48203 for funding.

REFERENCES

Ames, G. F.-L. (1986) *Annu. Rev. Biochem. 55,* 397−425.

Babu, Y. S., Bugg, C. E., & Cook, W. J. (1988) *J. Mol. Biol. 204*, 191−204.
Brito, R. M. M., Putkey, J. A., Strynadka, N. C. J., James, M. N. G., & Rosevear, P. R. (1991) *Biochemistry 30*, 10236−10245.
Brittain, H. G., Richardson, F. S., & Martin, R. B. (1976) *J. Am. Chem. Soc. 98*, 8255−8260.
Burroughs, S. E., Horrocks, W. D., Ren, H., & Klee, C. B. (1994) *Biochemistry 33*, 10428−10436.
Chao, S. H., Suzuki, Y., Zysk, J. R., & Cheung, W. Y. (1984) *Mol. Pharmacol. 26*, 75−82.
Chattopadhyaya, R., Meador, W. E., Means, A. R., & Quiocho, F. A. (1992) *J. Mol. Biol. 228*, 1177−1192.
Corson, D. C., Williams, T. C., & Sykes, B. D. (1983) *Biochemistry 22*, 5882−5889.
Cronce, D. T., & Horrocks, W. D. (1992) *Biochemistry 31*, 7963−7969.
da Silva, A. C. R., Kendrick-Jones, J., & Reinach, F. C. (1995) *J. Biol. Chem. 270*, 6773−6778.
Drake, S. K., & Falke, J. J. (1996) *Biochemistry 35*, 1753−1760.
Evans, C. H. (1990) *Biochemistry of the Lanthanides*, of the series *Biochemistry of the Elements*, Vol. 8, Plenum Press, New York.
Falke, J. J., Snyder, E. E., Thatcher, K. C., & Voertler, C. S. (1991) *Biochemistry 30*, 8690−8697.
Falke, J. J., Drake, S. K., Hazard, A. L., & Peersen, O. B. (1994) *Q. Rev. Biophys. 27*, 219−290.
Hapak, R. C., Lammers, P. J., Palmisano, W. A., Birnbaum, E. R., & Henzl, M. T. (1989) *J. Biol. Chem. 264*, 18751−18760.
Harned, H. S., & Owen, B. B. (1950) *Physical Chemistry of Electrolytic Solutions*, Reinhold Publishing Corp., New York.
Herzberg, O., & James, M. N. G. (1988) *J. Mol. Biol. 203*, 761−779.
Horrocks, W. D., & Albin, M. (1984) *Prog. Inorg. Chem. 31*, 1−104.
Kawasaki, H., & Kresinger, R. H. (1994) *Protein Profiles 1*, 343−517.
Kretsinger, R. H., & Nockolds, C. E. (1973) *J. Biol. Chem. 248*, 3313−3326.
Kumar, V. D., Lee, L., & Edwards, B. F. P. (1990) *Biochemistry 29*, 1404−1412.
Linse, S., & Forsen, S. (1995) *Adv. Second Messenger Phosphoprotein Res. 30*, 89−151.
MacManus, J. P., Hutnik, C. M. L., Sykes, B. D., Szabo, A. G., Williams, T. C., & Banville, D. (1989) *J. Biol. Chem. 264*, 3470−3477.
Marsden, B. J., Shaw, G. S., & Sykes, B. D. (1990) *Biochem. Cell Biol. 68*, 587−601.
Needham, J. V., Chen, T. Y., & Falke, J. J. (1993) *Biochemistry 32*, 3363−3367.
Park, C.-S., & MacKinnon, R. (1995) *Biochemistry 34*, 13328−13333.
Renner, M., Danielson, M. A., & Falke, J. J. (1993) *Proc. Natl. Acad. Sci. U.S.A. 90*, 6493−6497.
Sandberg, W. S., & Terwilliger, T. C. (1991) *Trends Biotechnol. 9*, 59−63.
Skelton, N. J., Kördel, J., Akke, M., Forsén, S., & Chazin, W. J. (1994) *Nature Struct. Biol. 1*, 239−245.
Snyder, E. E., Buoscio, B. W., & Falke, J. J. (1990) *Biochemistry 29*, 3937−3943.
Strynadka, N. C. J., & James, M. N. G. (1989) *Annu. Rev. Biochem. 58*, 951−998.
Tsien, R. W., & Tsien, R. Y. (1990) *Annu. Rev. Cell Biol. 6*, 715−760.
Wang, C.-L. A., Leavis, P. C., & Gergely, J. (1984) *Biochemistry 23*, 6410−6415.
Willians, T. C., Corson, D. C., & Sykes, B. D. (1984) *J. Am. Chem. Soc. 106*, 5698−5702.
Vyas, N. K., Vyas, M. N., & Quiocho, F. A. (1987) *Nature 327*, 635−638.
Vyas, M. N., Jacobson, B. L., & Quiocho, F. A. (1989) *J. Biol. Chem. 264*, 20817−20821.

BI952430L